



Design and catalytic studies of structural and functional models of the catechol oxidase enzyme

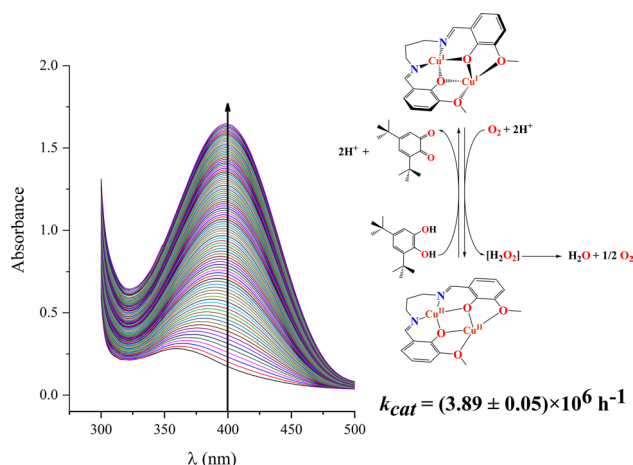
Aarón Terán¹ · Aida Jaafar¹ · Ana E. Sánchez-Peláez¹ · M. Carmen Torralba¹ · Ángel Gutiérrez¹

Received: 10 February 2020 / Accepted: 24 April 2020
© Society for Biological Inorganic Chemistry (SBIC) 2020

Abstract

The catechol oxidase activity of three copper/bicompartamental *salen* derivatives has been studied. One mononuclear, [CuL] (**1**), one homometallic, [Cu₂L(NO₃)₂] (**2**), and one heterometallic, [CuMnL(NO₃)₂] (**3**) complexes were obtained using the ligand H₂L = *N,N'*-bis(3-methoxysalicylidene)-1,3-propanediamine through different synthetic methods (electrochemical, chemical and solid state reaction). The structural data indicate that the metal ion disposition models the active site of *type-3* copper enzymes, such as catechol oxidase. In this way, their ability to act as functional models of the enzyme has been spectrophotometrically determined by monitorization of the oxidation of 3,5-di-*tert*-butylcatechol (3,5-DTBC) to 3,5-di-*tert*-butyl-*o*-benzoquinone (3,5-DTBQ). All the complexes show significant catalytic activity with ratio constants (k_{obs}) lying in the range $(223\text{--}294) \times 10^{-4} \text{ min}^{-1}$. A thorough kinetic study was carried out for complexes **2** and **3**, since they show structural similarities with the catechol oxidase enzyme. The greatest catalytic activity was found for the homonuclear dicopper compound (**2**) with a turnover value (k_{cat}) of $(3.89 \pm 0.05) \times 10^6 \text{ h}^{-1}$, which it is the higher reported to date, comparable to the enzyme itself ($8.25 \times 10^6 \text{ h}^{-1}$).

Graphic abstract



Keywords Catalytic activity · Biomimetic catalysis · Cu(II) complexes

Dedicated to Professor José Antonio Campo Santillana, in memoriam.

Electronic supplementary material The online version of this article (<https://doi.org/10.1007/s00775-020-01791-2>) contains supplementary material, which is available to authorized users.

Extended author information available on the last page of the article

Introduction

In last decades, one of the main purposes in bioinorganic chemistry was the focus on the synthesis and study of chemical models which were able to mimic the structure and function of the enzyme active sites using coordination chemistry

compounds [1]. Those models are simpler and, therefore, easy to study the relationship between structure and enzymatic function to establish a mechanism of the catalytic processes. Besides, in several cases, some of these reactions can be implemented in the industry with an adequate catalyst obtaining compounds under “greener” conditions [2].

Catechol oxidase enzyme is present in plants, animals, fungi and bacteria. It takes part in the conversion of a large number of *o*-catechols into the respective *o*-benzoquinones, which subsequently auto-polymerize, resulting in the formation of melanin, a dark pigment thought to protect a damaged tissue from pathogens. This enzyme is also relevant in the industry because of its uses as O₂ activator [2–4] or in medical diagnosis of human brain diseases (detection of catecholamines, noradrenaline and dopa in neurological disorders) [5].

The *type-3* active site of the enzyme consists of a dinuclear copper center where each copper is coordinated by three histidine nitrogen atoms and one hydroxo bridge, in the native *met* state [6]. Since the discovery of the nature of this active site, a great number of dicopper(II) complexes have been designed to mimic the structure and function of the enzyme [7].

The Schiff base-type ligands provide great environments to obtain dinuclear copper(II) complexes. In particular, bicompartamental *salen* (*N,N'*-disalicylideneethylenediamine) and its derivatives can be easily synthesized by condensation of an aldehyde or ketone with a primary amine [8]. Several modifications can be introduced in this type of ligands to modify their electronic and structural properties such as flexibility, electronic nature or steric characteristics resulting in an exceptionally rich coordination chemistry [9–11].

The best catechol oxidase model reported to date with copper complexes exhibit k_{cat} values around 10^4 h^{-1} , at least two orders of magnitude lower than those of the enzymes isolated from different sources ($k_{\text{cat}} = 8.25 \times 10^6 \text{ h}^{-1}$ from *Ipomoea batatas* (sweet potatoes) [12] and $k_{\text{cat}} = 5.7 \times 10^5 \text{ h}^{-1}$ from *Lycopus europaeu* [13]). In that sense, due to the great importance of this enzyme, it is of big interest to develop new models in order of improving their catecholase activity.

In this work, we report the synthesis and structural characterization of three structural model complexes of catechol oxidase enzyme obtained using one symmetric bicompartamental Schiff base ligand (*N,N'*-bis(3-methoxysalicylidene)-1,3-propanediamine, H₂L). This ligand has an inner site, N₂O₂, formed by two imines and two phenol groups and one outer site, O₂O₂, from the two bridging phenol groups and two methoxy groups in 3,3' positions (Fig. 1a). The inner site is more suitable to accommodate *3d* metal ions [14–19], while the external one is capable to accept diverse metal ions such as alkali [20], alkali earth [21], transition metals [22, 23] and lanthanides [24–26] as well as small molecules like water [27, 28] or ammonium cation [29]. We have also studied the catalytic activity of these complexes to check whether they can act not only as structural model but as functional models of the enzyme. The studies have been carried out using UV–Vis spectroscopy to follow the oxidation process of 3,5-di-*tert*-butylcatechol (3,5-DTBC) to 3,5-di-*tert*-butyl-*o*-benzoquinone (3,5-DTBQ) in an aerobic methanolic solution buffered at pH 8.

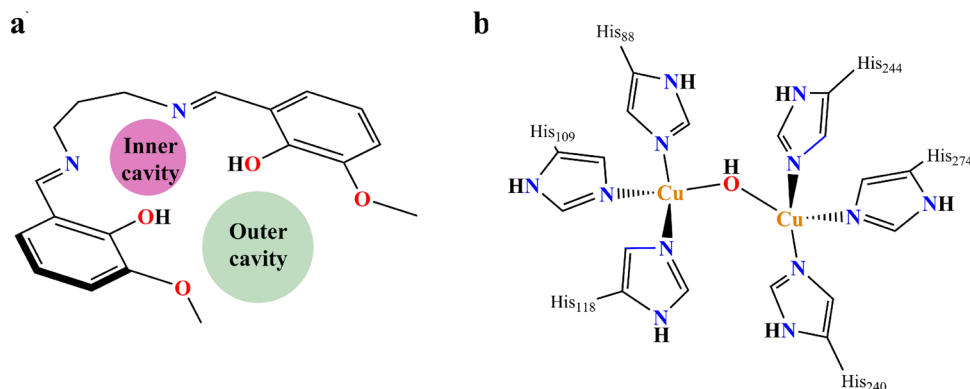
Materials and methods

Synthesis of complexes

Synthesis of H₂L

This ligand H₂L, (*N,N'*-bis(3-methoxysalicylidene)-1,3-propanediamine), was obtained by previously reported procedures [30]. A mixture of 3-methoxy-2-hydroxybenzaldehyde (4.30 g, 28 mmol) and 1,3-diaminopropane (1.2 mL, 14 mmol) in methanol (20 mL) by refluxing for 6 h. A yellow powder appears on cooling. The solid was filtered off, washed with methanol and air-dried. Yield 3.67 g (77%). Anal. C₁₉H₂₂N₂O₄ (342.39 g mol⁻¹) Calcd (%): C, 66.65; H, 6.48; N, 8.18. Found (%): C, 66.27; H, 6.32; N, 8.19. IR (cm⁻¹): 3421, 2940, 2948, 2902, 2880, 2839, 1631, 1491, 1469, 1441, 1414, 1384, 1359, 1337, 1271, 1256, 1171, 1129, 1095, 1081, 1051, 1032, 1006, 975, 961, 881,

Fig. 1 Coordination environment resemblance between the bicompartamental ligand H₂L (**a**) and the active site of catechol oxidase enzyme (**b**)



837, 785, 742, 730, 623, 570, 507. $^1\text{H-NMR}$ (300 MHz, CDCl_3): $\delta = 13.92$ ppm (s, 2H, **OH**), $\delta = 8.37$ ppm (s, 2H, **CH=N**), $\delta = 7.25$ – 6.80 ppm (m, 6H, **ArH**), $\delta = 3.91$ ppm (s, 6H, **OCH₃**), $\delta = 3.76$ – 3.71 ppm (td, 4H, **N-CH₂**), $\delta = 2.16$ – 2.06 ppm (q, 2H, **CH₂-CH₂-CH₂**). UV–Vis (CH_3OH): $\lambda_{\text{max}}/\text{nm}$ ($\epsilon/\text{dm}^3 \text{mol}^{-1} \text{cm}^{-1}$) = 263 (15,280), 296 (6196), 326 (3324), 420 (3321).

Synthesis of [CuL] (1)

H_2L (0.66 g, 2 mmol) was dissolved in methanol (140 mL) and placed in an electrochemical cell with a sacrificial copper anode and an inert platinum cathode using Et_4NBr as electrolyte. The intensity value was set up at 40 mA and the output was 100 V. The reaction time was 2 h and 41 min at room temperature. The green solid obtained was filtered off, methanol washed and vacuum dried. The E_f value was 0.5 mol F^{-1} which corresponds to the oxidation of metallic copper to Cu(II). Yield 0.48 g (60%). Anal. $\text{C}_{19}\text{H}_{20}\text{CuN}_2\text{O}_4$ ($403.90 \text{ g mol}^{-1}$) Calcd (%): C, 56.50; H, 4.99; N, 6.94. Found (%): C, 56.42; H, 4.91; N, 6.94. IR (cm^{-1}): 3431, 3053, 2999, 2941, 2830, 1629, 1545, 1471, 1441, 1403, 1327, 1243, 1221, 1167, 1101, 1082, 1008, 977, 959, 939, 857, 786, 743, 619, 560, 452. UV–Vis (CH_3OH): $\lambda_{\text{max}}/\text{nm}$ ($\epsilon/\text{dm}^3 \text{mol}^{-1} \text{cm}^{-1}$) = 282 (24,773), 371 (7172), 550 (197).

Synthesis of [Cu₂L(NO₃)₂] (2)

Three different procedures have been followed for the synthesis of the title compound.

- (i) A methanolic solution (40 mL) of $\text{Cu}(\text{NO}_3)_2 \cdot 3\text{H}_2\text{O}$ (0.80 g, 3.3 mmol) was added to an stirring solution of H_2L (0.36 g, 1.1 mmol) in methanol (15 mL). The reaction mixture was stirred at room temperature for 12 h. The solid appeared as a brown powder that was filtered off and washed with methanol. Single crystals suitable for X-ray data collection were obtained by slow evaporation of the filtered solution. Yield 0.41 g (65%).
- (ii) H_2L (0.17 g, 0.5 mmol) and $\text{Cu}(\text{NO}_3)_2 \cdot 3\text{H}_2\text{O}$ (0.14 g, 0.56 mmol) were dissolved in methanol (105 mL) in an electrochemical cell with a sacrificial copper anode and an inert platinum cathode. The intensity value was set up at 40 mA and the output was 100 V. The reaction time was 41 min at room temperature. The product was filtered off, washed with methanol and dried. The E_f value was 0.5 mol F^{-1} . Yield 0.13 g (43%).
- (iii) A solid mixture of $\text{Cu}(\text{NO}_3)_2 \cdot 3\text{H}_2\text{O}$ (0.10 g, 0.4 mmol) and H_2L (0.14 g, 0.4 mmol) was ground for 30 min at room temperature. The mixture was suspended in methanol to extract the excess of re-

agents and leaving the product as a brown solid, which was filtered, washed with cold methanol and dried over P_4O_{10} . Yield 0.12 g (52%).

Anal. $\text{C}_{19}\text{H}_{20}\text{Cu}_2\text{N}_4\text{O}_{10}$ ($591.47 \text{ g mol}^{-1}$) Calcd (%): C, 38.12; H, 3.50; N, 9.36. Found (%): C, 37.82; H, 3.34; N, 9.26. IR (cm^{-1}): 2993, 2949, 2925, 1627, 1613, 1559, 1519, 1494, 1477, 1466, 1440, 1422, 1409, 1384, 1353, 1335, 1307, 1297, 1245, 1233, 1199, 1173, 1101, 1079, 1070, 1015, 1011, 990, 983, 955, 934, 894, 855, 839, 805, 784, 762, 745. UV–Vis (CH_3OH): $\lambda_{\text{max}}/\text{nm}$ ($\epsilon/\text{dm}^3 \text{mol}^{-1} \text{cm}^{-1}$) = 226 (47,027), 279 (24,284), 360 (6360), 608 (78).

Synthesis of [CuMnL(NO₃)₂] (3)

This compound has been prepared following the previously reported procedure [22]. The mononuclear complex (1) (0.10 g, 0.5 mmol) was dissolved in $\text{MeOH}:\text{MeCN}$ (1:4) (125 mL), $\text{Mn}(\text{NO}_3)_2 \cdot 4\text{H}_2\text{O}$ (0.06 g, 0.5 mmol) was added and the resulting solution was stirred for 0.5 h. After 4 days of slow evaporation at low temperature, a dark green powder and single crystals suitable for X-ray data collection were obtained. The product was filtered off, washed with cold methanol and dried in vacuum. Yield 0.19 g (66%). Anal. $\text{C}_{19}\text{H}_{20}\text{CuMnN}_4\text{O}_{10}$ ($582.87 \text{ g mol}^{-1}$) Calcd (%): C, 39.15; H, 3.46; N, 9.61. Found (%): C, 39.36; H, 3.58; N, 9.27. IR (cm^{-1}): 1617, 1561, 1472, 1445, 1384, 1302, 1236, 1172, 1101, 1073, 1030, 988, 953, 855, 786, 745, 638, 574, 539, 466. UV–Vis (CH_3OH): $\lambda_{\text{max}}/\text{nm}$ ($\epsilon/\text{dm}^3 \text{mol}^{-1} \text{cm}^{-1}$) = 226 (44,254), 276 (19,559), 356 (4630), 618 (33).

Physical methods and materials

All chemicals of analytical grade were purchased from Sigma-Aldrich and used without further purification.

Elemental analysis (carbon, hydrogen and nitrogen) were carried out by the Microanalytical Service of the Universidad Complutense de Madrid (UCM) using a LECO CHNS-932 analyser. FTIR spectra (4000 – 650 cm^{-1}) of solid powder samples were recorded using a Perking Elmer spectrophotometer with a universal ATR accessory and FTIR KBr-dispersion spectra (4000 – 400 cm^{-1}) were recorded using a THERMO NICOLET 200 spectrophotometer. Mass spectra were recorded using electrospray ionization (ESI–MS) in DMSO and MeOH with the HCTultraPTM Discovery System mass spectrometer equipped with a conventional ESI source. $^1\text{H-NMR}$ spectra were collected in the UCM Nuclear Magnetic Resonance Service using a Burkner AVIII300 (300 MHz) spectrophotometer. Electronic spectra in oxygenated methanol (200 – 1000 nm) were registered in a Cary-5G spectrophotometer. The measurements of the catalytic oxidation of 3,5-di-*tert*-butylcatechol (3,5-DTBC) were carried

out in a JASCO V-630 spectrophotometer at a constant wavelength of 400 nm under aerobic conditions at 20 °C and in buffered solution at pH 8 with tris(hydroxymethyl)aminomethane (Tris). Variable-temperature magnetic susceptibility measurements in the temperature range 2–300 K were performed on a Quantum Design MPMSXL SQUID magnetometer using a constant magnetic field of 0.5 T. All susceptibility data were corrected for the diamagnetic contribution of the sample holder, while the molar diamagnetic corrections from the sample were calculated using the Pascal constants. Cyclic voltammetry (CV) measurements were performed using an EmStat3 blue potentiostat controlled by PSTrace software. A three-electrode assembly comprising a gold working electrode, platinum auxiliary electrode and Ag/AgCl electrode as reference electrode were used. The cyclic voltammetry study was carried out at room temperature in MeCN:H₂O (2:1) solution under Argon with 50 mM Tris buffer (pH 8) at a scan rate of 50 mV s⁻¹ in a potential range from +0.8 to -0.8 V.

Crystallographic studies

A good quality crystal of (**2**) was directly collected from the reaction vessel and mounted on a Bruker Smart-CCD diffractometer using graphite monochromated Mo K α radiation ($\lambda = 0.71073$ Å) operating at 50 kV and 25 mA at 293 K. Data were collected over a reciprocal space hemisphere by combination of three exposure sets. Each frame exposure time was 20 s covering 0.3° in ω . The cell parameters were determined and refined by least-squares fit of all reflections collected. The first 50 frames were recollected at the end of the data collection to monitor crystal decay, and no appreciable decay was observed. The structure was solved by direct methods and refined by applying full-matrix least-squares on F^2 with anisotropic thermal parameters for the non-hydrogen atoms. The hydrogen atoms were included with fixed isotropic contributions at their calculated positions determined by molecular geometry. All the calculations were carried out using SHELXT program for solution and SHELXL for refinement [31] working into the OLEX2 software package program [32]. A summary of the fundamental data can be found in the supplementary material Table S1.

Catalytic activity and kinetic studies

Catecholase-like activity and kinetic studies of complexes **1–3** were evaluated in aerobic condition spectrophotometrically by monitoring the oxidation of 3,5-DTBC to 3,5-DTBQ at 400 nm as a function of time. The reaction was studied in a thermostated cell with 1 cm path length at 20.0 ± 0.1 °C. The solvent used to prepare all solutions was Tris buffer (100 mM, pH 8) in methanol medium saturated with atmospheric dioxygen during several minutes.

For catalytic activity studies, 2×10^{-5} M solutions of complexes **1–3** were treated with 2×10^{-3} M solutions of the substrate 3,5-DTBC. The reaction progress was followed by UV/Vis spectroscopy observing the increase in the characteristic quinone (3,5-DTBQ) absorption band at 400 nm. The data were taken at intervals of 60 s and the conversion was measured up to 60 min in each case. All data were fixed to a first-order kinetic according to Eq. (1), where A_∞ denotes absorbance at $t = \infty$, A_t is the variation absorbance value with time and k_{obs} is the rate constant.

$$\log \left(\frac{A_\infty}{A_\infty - A_t} \right) = k_{\text{obs}} \cdot t. \quad (1)$$

Enzymatic kinetic experiments for the oxidation of 3,5-DTBC to 3,5-DTBQ were performed using complex **2** and **3** as catalysts. The experimental procedure was carried out by the initial rate method monitoring by UV-Vis spectroscopy. The experiments were carried out by keeping constant the final catalyst concentration at 2×10^{-5} M and changing the substrate concentration between 2×10^{-3} and 2×10^{-2} M.

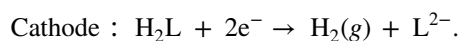
Results and discussion

Synthesis of complexes

The synthetic procedures followed in this work are summarized in Scheme 1.

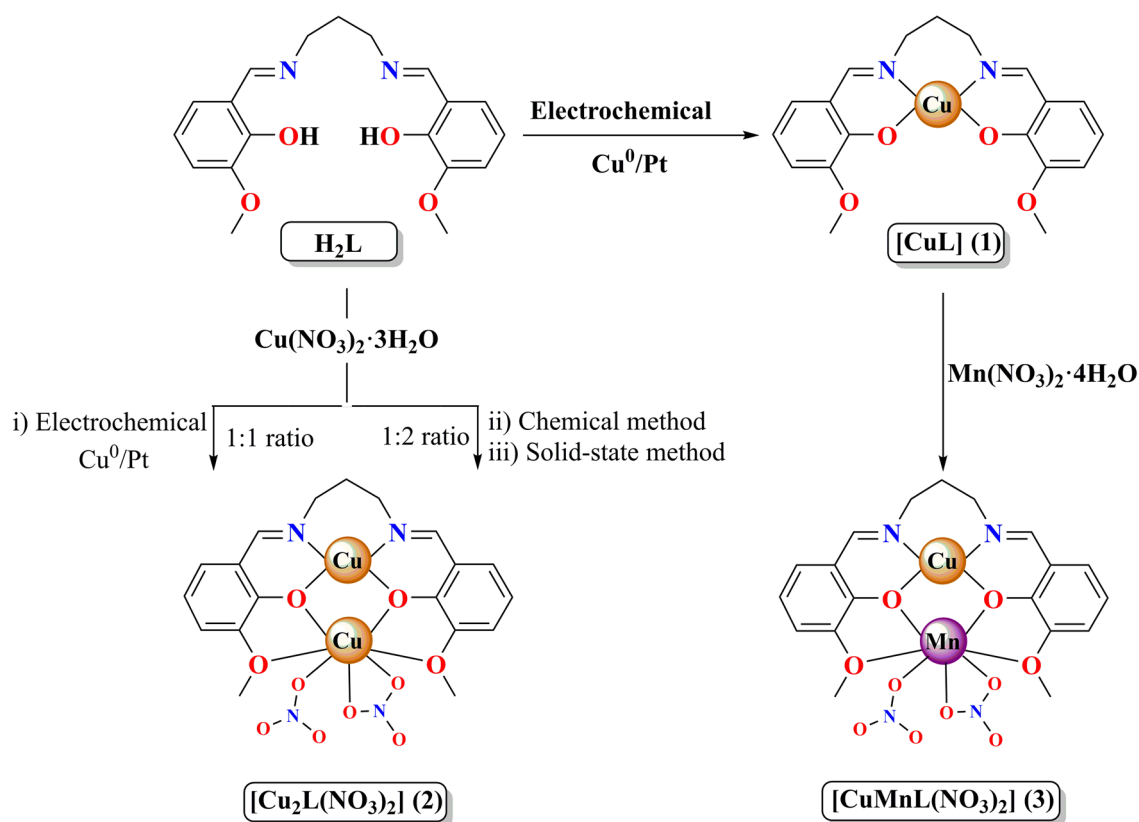
The mononuclear complex [CuL] (**1**) has been obtained by an electrochemical procedure, an unusual synthetic route for this type of compound, where a copper wire electrode is oxidized by an electric current to form copper(II) ions that coordinate into the inner cavity of the anionic bicompartimental ligand. This procedure allows a precise stoichiometric control of the reacting copper(II) amount, obtaining purer derivatives with a lower formation of by-products.

The efficiency of the electrochemical process is 0.5 mol F⁻¹, indicative of a two electron transfer according to the following half-reactions:



The homonuclear [Cu₂L(NO₃)₂] (**2**) has been synthesized by three different routes:

- (i) electrochemical synthesis in presence of excess Cu(NO₃)₂·3H₂O;
- (ii) one-pot chemical reaction by mixing methanolic solutions of H₂L and Cu(NO₃)₂·3H₂O in a 1:2 stoichiometric ratio;



Scheme 1 Synthetic routes used for the preparation of complexes 1–3

- (iii) solid state grinding of H_2L and $Cu(NO_3)_2 \cdot 3H_2O$ in a 1:2 ratio.

All procedures lead to similar results in purity and yield of the dinuclear derivative.

The heteronuclear derivative, **3**, can only be obtained in good yields by reaction of methanolic solutions of **1** with $Mn(NO_3)_2 \cdot 4H_2O$. The use of other synthetic procedures lead to a competition between the Cu(II) and Mn(II) ions to occupy the coordinative cavities of the *salen* ligand, the main product being **2**.

Infrared spectra

The IR spectra indicate that the coordination of a metal center to the *salen* ligand slightly shifts the characteristic vibration bands, $\nu(C=N) = 1630\text{ cm}^{-1}$, $\nu(C-O)_{\text{phenoxo}} = 1255\text{ cm}^{-1}$ and $\nu_s(C-OCH_3) = 1081\text{ cm}^{-1}$. Thus, these bands appear respectively at 1629, 1239 and 1070 cm^{-1} for **1**, 1613, 1245 and 1070 cm^{-1} for **2** and 1617, 1246 and 1070 cm^{-1} for **3**. The shift to lower frequencies is indicative of the lower electron density on the donor atoms because of the coordination of the metal atoms [33]. The two latter compounds also show characteristic bands around 1470, 1310 and 1030 cm^{-1}

associated to $\nu(N=O)$, $\nu_{\text{as}}(NO_2)$ and $\nu_s(NO_2)$, respectively, which are indicative of the presence of coordinated nitrate groups [34] (see supplementary material Figure S1).

Electronic spectra

The electronic spectrum for the ligand, H_2L , shows three bands in the 260–330 nm region that are ascribed to intraligand $\pi \rightarrow \pi^*$ and $n \rightarrow \pi^*$ transitions. Additionally, the ligand shows an intense absorption band at 420 nm, assigned to a charge transfer between the ligand and the methanol solvent (MSCT), since this band was not observed when the spectra were collected in acetonitrile solution. The formation of the complexes causes a bathochromic shift of the intraligand transitions along with the appearance of a low-intensity absorption band centred at 600 nm that can be assigned to a $d-d$ transition for the copper(II) ion due to the ${}^2T_{2g} \leftarrow {}^2E_{2g}$ transition. In the dinuclear complexes, a charge transfer between the metal ion and the ligand (MLCT) at about 360 nm for **2** and 356 nm for **3** is also observed. A broad low-intensity absorption band at 608 nm for the Cu–Cu complex and 618 nm for the Cu–Mn one is also attributed to the $d-d$ transition of the copper(II) ion [35] (see supplementary material Figure S2).

X-ray crystal structure of (2)

Single crystals suitable for X-ray diffraction have been obtained from methanolic solutions of the dinuclear complexes.

The crystal structure of **2** indicates that it is isomorphous with the previously characterized complex **3** (Fig. 2) [22]. Both complexes show a copper(II) ion coordinated to the inner cavity, N_2O_2 , in a square-planar geometry. The presence of a second coordination site, O_2O_2 , allows the coordination of a second metal ion, copper(II) in **2** or manganese(II) in **3**. In both cases, this ion is heptacoordinated by the four oxygen atoms from the outer site of the ligand and by three oxygen atoms from two nitrate anions, in a bidentate and monodentate fashion. The bond distances between the copper ion and the donor atoms in the inner cavity are very similar, about 1.9 Å, in both complexes. The difference in size of the metal ion located in the outer cavity

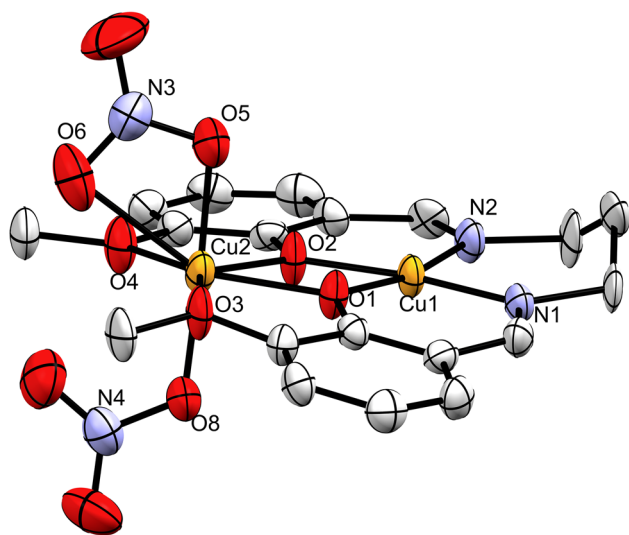


Fig. 2 ORTEP view (50% probability ellipsoids) and labelling scheme of the asymmetric unit for **2**

results in small differences in the metal–oxygen distances (2.41–2.42 Å for the Cu–Cu derivative and 2.37–2.38 Å for the Cu–Mn one), leading to metal–metal separations of $Cu\cdots Cu = 3.232(1)$ Å and $Cu\cdots Mn = 3.322(1)$ Å, respectively. The former distance is very similar to the $Cu\cdots Cu$ distance observed in the *met* state of catechol oxidase enzyme (3.032 Å). A comparison between the coordinative environment of the dinuclear complexes and that of the active site of *met* state of this enzyme is observed in Fig. 3.

Magnetic properties

The magnetic susceptibility data for **2** and **3** have been measured in the temperature range 2–200 and 2–300 K, respectively. The temperature dependence of the χT values has been plotted in Fig. 4 for the two complexes.

The high temperature value of χT for **2** (Fig. 4a) is $0.554 \text{ cm}^3 \text{ K mol}^{-1}$, below the expected value for two isolated $S = 1/2$ spins ($0.75 \text{ cm}^3 \text{ K mol}^{-1}$). On cooling, the χT values decrease to a minimum value of $0.343 \text{ cm}^3 \text{ K mol}^{-1}$ at 2 K. This behaviour can be interpreted in terms of an antiferromagnetic coupling between the two copper(II) ions in the same molecular unit. In this sense, the magnetic data for the dicopper complex have been fitted to Heisenberg's dimers model according to Hamiltonian $H = -J \cdot S_1 \cdot S_2$, where J is the coupling constant between both spins, with the addition of a temperature independent paramagnetism term. The best fit (solid line) was obtained when $g = 2.305(2)$, $J = -1.45(3) \text{ cm}^{-1}$ and $N\alpha = 2.7(1) \times 10^{-4} \text{ cm}^3 \text{ mol}^{-1}$, this results agree with the antiferromagnetic behaviour between the two metal ions.

Compound **3** shows a similar behaviour (Fig. 4b), with a room temperature χT value at of $3.99 \text{ cm}^3 \text{ K mol}^{-1}$, lower than the expected for one $S = 1/2$ and one $S = 5/2$ independent spins ($4.38 \text{ cm}^3 \text{ K mol}^{-1}$). The χT values decrease on cooling until ca. 40 K, when they reach a plateau at $2.89 \text{ cm}^3 \text{ K mol}^{-1}$, very close to the expected value of $3.00 \text{ cm}^3 \text{ K mol}^{-1}$ for the two spins coupling antiferromagnetically. Below 15 K, the χT values decrease once more to a minimum value of 2.47

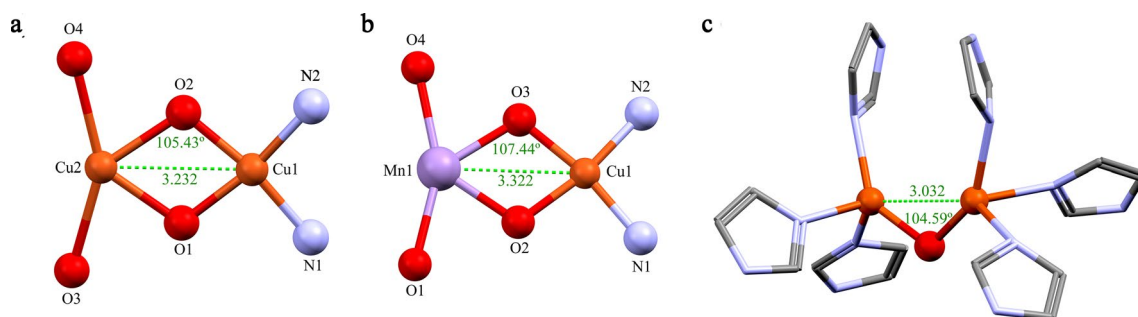
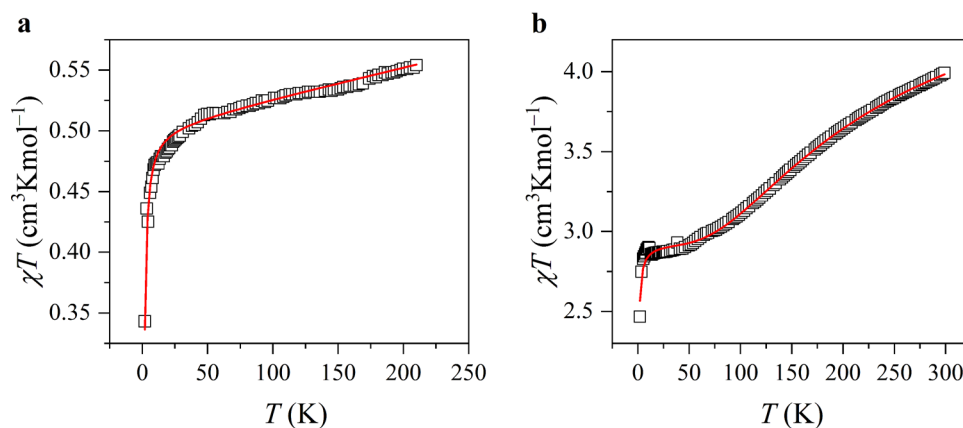


Fig. 3 Metal–metal distances and angles of dinuclear complexes, **2** (a) and **3** (b), and the coordination sphere of the dinuclear copper(II) centre of catechol oxidase from sweet potato in the *met* state (PDB ID: 1BT3) (c)

Fig. 4 Temperature dependence of χT for complexes **a** and **b**. The solid lines represent the fit of the data using the parameters described in the text



$\text{cm}^3 \text{Kmol}^{-1}$ at 2 K; this fact can be attributed to the zero field splitting of the manganese ion, observable at very low temperatures, indicative of a small anisotropy distortion in the metal environment. To simplify the fitting, we have treated the data in two steps:

The evaluation of the zero field splitting contribution for the manganese has been evaluated by fitting the data below 30 K, with the use of the Hamiltonian $H = D \cdot S_z^2$, where D is the zero field splitting parameter for the manganese ion. The best fit corresponds to $g_{\text{Mn}} = 1.962(2)$ and $D = 1.52(7) \text{ cm}^{-1}$.

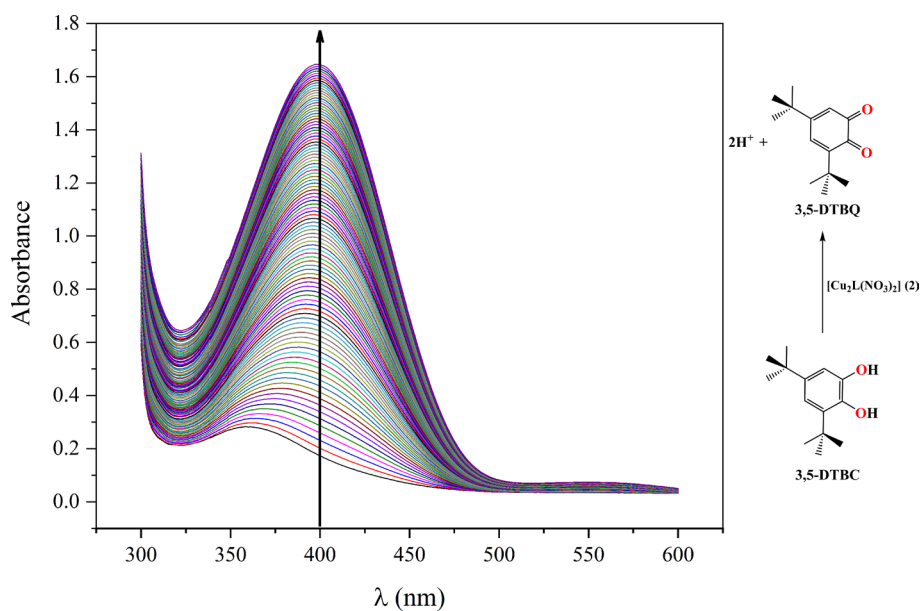
In a second step, the whole set of data were fitted, using a Heisenberg's dimers model and the zero field splitting correction for the Mn(II) cation anisotropy, along with a temperature independent paramagnetism term, usually present when the Cu(II) ion is involved. The resulting Hamiltonian was $H = -J \cdot S_{\text{Cu}} \cdot S_{\text{Mn}} + D \cdot S_z^2$, where J is the coupling constant between copper and manganese ions. The g_{Mn} and

D values obtained from the previous fitting were kept constant and the fit (solid line in Fig. 3) affords the final values $g_{\text{Cu}} = 2.350(2)$, $J = -70.6(5) \text{ cm}^{-1}$ and $N\alpha = 4.6(2) \times 10^{-4} \text{ cm}^3 \text{ mol}^{-1}$, as expected for the antiferromagnetic coupling predicted between the two metal spins.

Catechol oxidase activity

The synthesized complexes in this research have been designed as structural and functional models of the catechol oxidase enzyme, so it is necessary to evaluate their ability to oxidize a catechol (3,5-DTBC) to the corresponding quinone (3,5-DTBQ). The reaction progress was followed by UV/Vis spectroscopy (Fig. 5) observing the increase in the characteristic quinone (3,5-DTBQ) absorption band at 400 nm as function of time in all three cases (see supplementary material Figure S3) [3, 36].

Fig. 5 Variation of 3,5-DTBQ absorbance at 400 nm after addition of complex **2**. The spectra were recorded at intervals of 60 s during 60 min



As a previous step, to take into account the possible autoxidation of the catechol, different blank experiments were performed. The autoxidation of the 3,5-DTBC substrate was measured in the absence of Tris buffer and without oxygenation of the solvent and checked that the autoxidation process does not occur if the medium has not been previously oxygenated and that the highest autoxidation rate was obtained when the pH was buffered at 8.

In all three complexes, the k_{obs} values for a first-order kinetic indicate a remarkable catalytic oxidation process to form the quinone (Table 1).

The obtained ratio constant values are of the same magnitude order, making difficult the identification of the complex having the best catalytic activity and the observation of what structural and compositional differences improve or fall away the catalytic process. For this reason, an evaluation of the conversion percentage of catechol to quinone was made to check which compound shows the best catalytic behaviour. To do this, a calibration curve was made using methanol-oxygenated 3,5-DTBC solutions buffered at pH 8 at three different concentrations, 0.005 M, 0.010 M and 0.015 M. The calibration plot allows the interpolation of the amount of quinone formed in the presence of the catalyst during the first 30 min of reaction. The UV–Vis absorbance at 400 nm for each solution was recorded after 24 h to ensure that all 3,5-DTBC had been converted to 3,5-DTBQ. The results are shown in Fig. 6.

The presence of any of the three metallic compounds improves the catalytic process relative to the autoxidation

process. The dinuclear compounds have a better catalytic activity than the mononuclear complex and the homonuclear dicopper derivative shows the best behaviour, since it is the most structural and compositionally analogous to the active site of catechol oxidase enzyme, which it is a *type-3* copper enzyme.

According to these results, the enzymatic kinetic study was carried out with the dinuclear compounds, **2** and **3**, because of their quick conversion processes. These compounds have been chosen to elucidate a possible mechanism involved in the catalytic process as well, using two analogue compounds that show differences in the composition of the active site.

Enzymatic kinetic experiments for the oxidation of 3,5-DTBC to 3,5-DTBQ were performed using **2** and **3** as catalysts, setting the final concentration at 2×10^{-5} M. The initial rate (V_0) is calculated for each substrate concentration (between 2×10^{-3} and 2×10^{-2} M) from the slope of the first-order fitting data at the beginning of the reaction (only the first three measurements), when the reverse reaction is insignificant.

The obtained data were analysed using the Michaelis–Menten approach of enzymatic kinetic. The kinetic parameters, V_{max} , K_M and k_{cat} , were calculated from the Lineweaver–Burk double reciprocal plot. The observed initial rate (V_0) versus the concentration of 3,5-DTBC plot and the Lineweaver–Burk plot for **2** and **3** are shown in Fig. 7.

The typical asymptotic representation of the Michaelis–Menten kinetic plot was not observed in Fig. 7a because the maximum rate, V_{max} , is not reached. This parameter represents the amount of substrate molecules converted into the product by an enzyme molecule per unit time when the enzyme is fully saturated with substrate, so in this case, the saturation of the catalysts is not achieved at the measured substrate concentrations indicating that the catalytic process must occur very quickly. The Michaelis constant (K_M), which it is inversely related with x -intercept of the graphs (Fig. 7b), represents the substrate concentration at

Table 1 Values of k_{obs} obtained using the complexes described in this work as catalysts

Catalyst	[C] (mol L ⁻¹)	k_{obs} (min ⁻¹)
1	2×10^{-5}	$(258 \pm 4) \times 10^{-4}$
2	2×10^{-5}	$(294 \pm 4) \times 10^{-4}$
3	2×10^{-5}	$(282 \pm 2) \times 10^{-4}$

Fig. 6 **a** Calibration curve of 3,5-DTBC. **b** Percentage conversion of 3,5-DTBC to 3,5-DTBQ in the presence of the catalysts, **1** (red), **2** (green), **3** (black) and autoxidation (blue) during the first 30 min reaction time

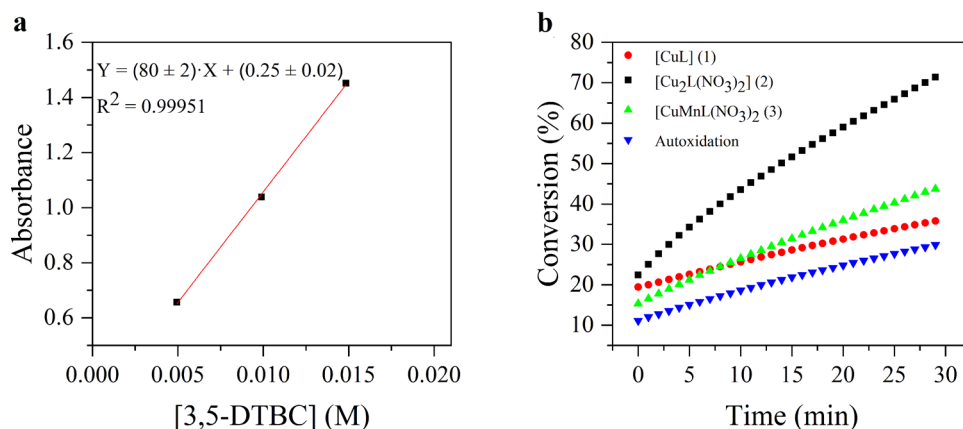


Fig. 7 **a** Plot of initial rate vs. substrate concentration for the oxidation of 3,5-DTBC by complexes **2** (red) and **3** (blue). **b** Lineweaver–Burk plot of complexes **2** (red) and **3** (blue)

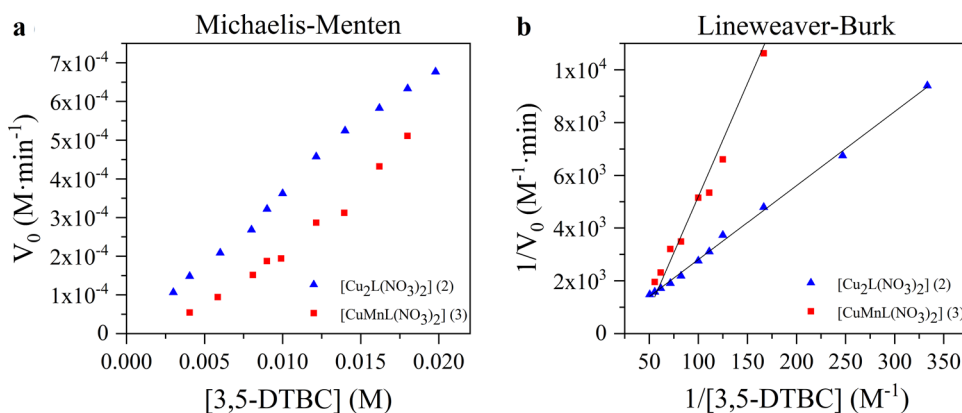


Table 2 Kinetic parameters for the dinuclear complexes as catalysts

[Catalyst] (M)	V_{\max} (M·min ⁻¹)	K_M (mM)	k_{cat} (h ⁻¹)	k_{cat}/K_M (mM ⁻¹ h ⁻¹)
2	0.039	36.6 ± 0.6	(3.89 ± 0.05) × 10 ⁶	106,059
3	0.003	25 ± 3	892 ± 7	36

half-maximum reaction rate and it is dependent on both the enzyme and the substrate, as well as on conditions such as temperature and pH. K_M is correlated with the dissociation constant of the enzyme–substrate complex, so a higher value means a low affinity in the enzyme–substrate complex.

The kinetic parameters for both complexes are summarized in Table 2. The higher K_M and k_{cat} values found for the dicopper derivative suggest the best catalytic behaviour for this compound.

A study of the pH influence on the catalytic process has been carried out for compound **2**. The enzymatic kinetic experiments were performed at pH 7 in the absence of buffer. In this case, the k_{cat} value obtained was (2.93 ± 0.03) × 10⁴ h⁻¹, one order of magnitude lower than in the buffered experiment. These kinetic parameters are consistent with an improvement of the catalytic activity associated with a greater substrate–catalyst affinity favoured by the coordination of the deprotonated catechol to the copper(II) metal ions. As observed in Fig. 8, there is a substantial increase of nearly 30% in the substrate oxidation after 30 min of reaction with the increase of pH.

Through comparison with published catalytic constant (K_M and k_{cat}) values for other metal compounds with similar catechol oxidase activity (summarized in Table 3), it is clear that **2** is one of the best catalyst models for this oxidation process and that the k_{cat} value is one of the highest reported, being comparable to that measured for the catechol oxidase enzyme.

This behaviour can be related to the fact that **2** is formed by a flexible ligand capable of accommodating two metal centers with a suitable Cu...Cu distance. One of these centers has coordinative vacancies while the other is coordinated to two nitrate ligands, easily displaced, favouring the

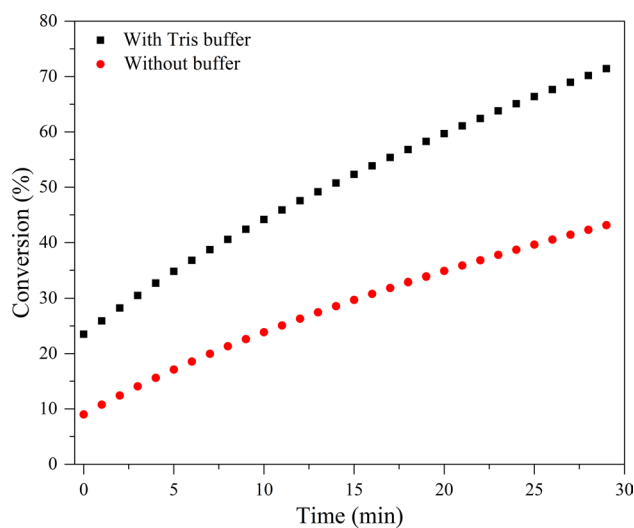


Fig. 8 Ratio of 3,5-DTBC conversion in Tris buffer medium (black) and without buffer (red) for **2**. Catalyst to 3,5-DTBC molar ratio 1:400

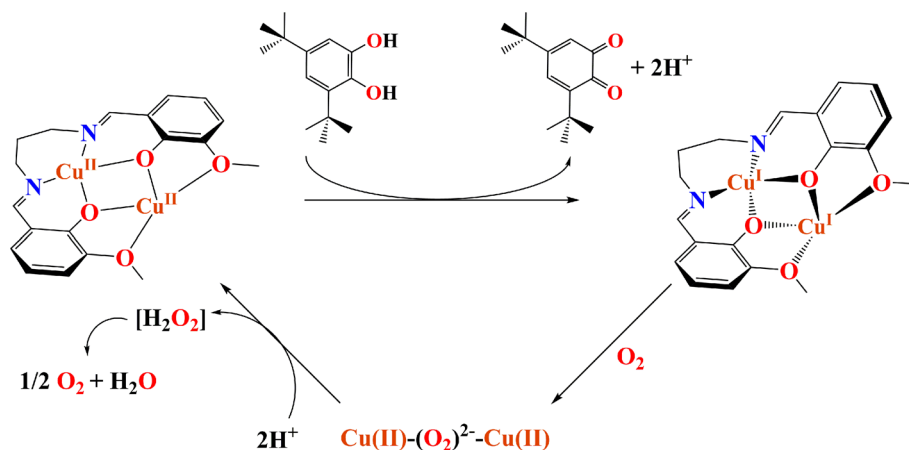
coordination of a bridging catechol molecule during the catalytic process.

In the case of the Cu–Mn compound, where the only difference with the dicopper complex is the presence of a manganese(II) atom of the outer cavity, the percentage conversion values are very low. So, it can be deduced that the presence, in the case of **3**, of a second metal ion does not have a prodigious influence on the catalytic process because of the low tendency of Mn(II) to be reduced, preventing a more efficient catalytic process.

A plausible mechanism for the catalytic process using complex **2** is given in Scheme 2. In a first step, the

Table 3 Values of K_M and k_{cat} reported for different compounds with Schiff base ligands showing catechol oxidase activity

Metal	Solvent	K_M (mM)	k_{cat} (h^{-1})	References
Dinuclear Ni(II)	[a]	0.3	1.44×10^4	[37]
Dinuclear Cu(II)	[a]	1.7–2.3	$(1.08–3.24) \times 10^4$	[38, 39]
	[b]	1.09–9.7	$(0.0167–2.16) \times 10^4$	
Dinuclear Mn(III)	[b]	0.9–3.7	$(2.41–3.60) \times 10^3$	[5]
Mononuclear Mn(III)	[b]	0.7–8.3	$(0.17–1.80) \times 10^4$	
	[a]	0.1–4.2	$(2.47–7.20) \times 10^3$	
Mononuclear Mn(II)	[c]	9.52	3.10×10^6	[40]
Dinuclear Cu(II) (2)	[a]	36.6	3.89×10^6	This work

[a] MeOH, [b] CH₃CN, [c] DMF**Scheme 2.** Proposed mechanism for the oxidation process of 3,5-DTBC to 3,5-DTBQ

3,5-DTBC displaces one nitrate ligand from the coordination sphere of the Cu(II) ion located in the outer cavity and coordinates to the two metal ions [6, 41, 42]. Electrospray ionization mass spectrometry (ESI-MS) measurements of compound **2** detected a peaks at $m/z = 232.9$ $[M - 2NO_3]^{2+}$, 271.9 $[M - 2NO_3 + DMSO]^{2+}$ and 527.9 $[M - NO_3]^+$ (see supplementary material Figure S5). In addition, the UV-Vis measurements indicate clear differences between the solution spectra of **1** and **2**. Both facts clearly demonstrate the stability of the dinuclear derivative, both in solid state and solution, and it can be assumed that the second metal ion remains stable on the ligand outer cavity, its presence being crucial in the catalytic process.

The oxidation process of 3,5-DTBC to 3,5-DTBQ by transfer of two electron from the two Cu(II)/Cu(II) active site causes their reduction to Cu(I)/Cu(I). Once the quinone is uncoordinated, the interaction with molecular O₂ from the reaction medium produces the reoxidation of the dimetallic core giving rise to water molecules and regenerating the catalyst. The catalytic mechanism described for the most compounds that have catechol oxidase activity shows the formation of hydrogen peroxide (H₂O₂) in the catalysis process [7]. In this case, an iodometry was carried out to detect H₂O₂ during the 3,5-DTBC oxidation but no hydrogen peroxide was observed. This fact can either indicate that

hydrogen peroxide was not formed and the reaction would directly proceed to the formation of water or, more probably in our opinion, that we were unable to detect the hydrogen peroxide since it would disproportionate very fast in the reaction media. According to the literature on the catalytic mechanism for cobalt and manganese compounds, the ROS-involved mechanism has not been probed overall and it is supported the formation of water [43–46]. This may be because Mn and Co compounds are remarkable for carrying out the fast decomposition of H₂O₂ which leads to the formation of H₂O and O₂ [47, 48]. Chaudhuri et al. showed that lowering temperature (– 25 °C) can help to slow down the decomposition of H₂O₂ allowing its detection [46].

Due to the ligand flexibility, a distortion of the coordination environment of the copper (inner or outer) from a square planar geometry to pseudo-tetrahedral is possible, through a rotation of the propylene spacer which it would facilitate the stabilization of Cu(I) ion. Cyclic voltammetric measurements have proven that the redox behaviour of **2** (Fig. 9) is reversible in the reaction conditions. The voltammogram plot shows two reduction peaks at – 0.01 V and – 0.63 V and two oxidation peaks at – 0.32 V and 0.08 V, respectively. These pseudo-reversible processes can be assigned to the successive reductions from Cu(II) to Cu(I) of the metal ions. The peak centred at 0.04 V would correspond to the

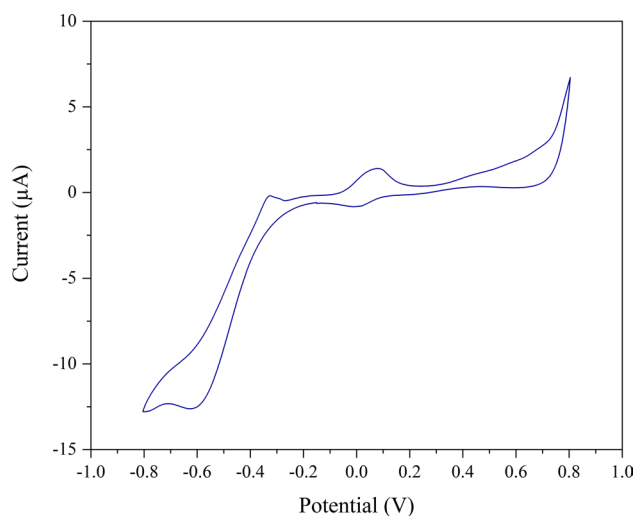


Fig. 9 Cyclic voltammogram of complex **2** in MeCN:H₂O (2:1) solution

copper located in the inner cavity, coordinated to stronger donor atoms, while the process centred at -0.47 V can be attributed to the metal ion in the outer (O_2O_2) cavity. This result suggests a redox behaviour for this species compatible with the activity of the catecholase metal site.

Conclusions

In summary, three complexes using a symmetrical bicompartamental Schiff base ligand, one mononuclear and two dinuclear (homo- or heterometallic) were synthesized, characterized and their catechol oxidase activity was studied. The catalytic activity of all three complexes was monitored by UV–Vis spectroscopy using the Michaelis–Menten approach to calculate their kinetic parameters complex. The obtained data suggest that the best catalytic behaviour was observed for the homonuclear derivative $[Cu_2L(NO_3)_2]$ (**2**) since this species provides the highest conversion rates and its k_{cat} value, $(3.89 \pm 0.05) \times 10^6$ h⁻¹, is the highest turnover number reported to date for this catalytic process. This excellent behaviour can be related to the structural similarities observed between the Cu–Cu active site of this compound and that of the catechol oxidase enzyme. This similarity allows us to propose for this catalytic process a mechanism similar to that reported for the enzyme.

Acknowledgements The authors gratefully acknowledge the Spanish Ministry of Economy and Competitiveness (MINECO/FEDER) for financial support (Project CTQ2015-63858-P) and Comunidad de Madrid (Project S2017/BMD-3770-CM). One of us (Aarón Terán) acknowledge Comunidad de Madrid (Project S2017/BMD-3770-CM) for a predoctoral Grant.

Compliance with ethical standards

Conflict of interest The manuscript was written through contributions of all authors. All authors have given approval to the final version of the manuscript. The authors declare no competing financial interest.

References

- Sureshbabu P, Junaid QM, Upadhyay C et al (2019) Di and tetranuclear Cu(II) complexes with simple 2-aminoethylpyridine: magnetic properties, phosphodiester hydrolysis, DNA binding/cleavage, cytotoxicity and catecholase activity. *Polyhedron* 164:202–218. <https://doi.org/10.1016/j.poly.2019.02.015>
- Garcia-Bosch I, Karlin KD (2014) Copper peroxide bioinorganic chemistry: from metalloenzymes to bioinspired synthetic systems. In: Rappoport Z (ed) *PATAI'S chemistry of functional groups*. Wiley, Chichester, 1–52. <https://doi.org/10.1002/9780470682531.pat0863>
- Neves A, Rossi LM, Bortoluzzi AJ et al (2002) Catecholase activity of a series of dicopper(II) complexes with variable Cu–OH(phenol) moieties. *Inorg Chem* 41:1788–1794. <https://doi.org/10.1021/ic010708u>
- Sathya V, Murali M (2018) Functional mimics of type-2 and type-3 copper oxidases: self-assembled molecular association in mononuclear copper(II) complex enhances the catalytic activity. *Inorg Chem Commun* 92:55–59. <https://doi.org/10.1016/j.inoch.2018.04.003>
- Banu KS, Chattopadhyay T, Banerjee A et al (2009) Mono- and dinuclear manganese(III) complexes showing efficient catechol oxidase activity: syntheses, characterization and spectroscopic studies. *Dalton Trans*. <https://doi.org/10.1039/b902498k>
- Klabunde T, Eicken C, Sacchettini JC, Krebs B (1998) Crystal structure of a plant catechol oxidase containing a dicopper center. *Nat Struct Biol* 5:1084–1090. <https://doi.org/10.1038/4193>
- Dey SK, Mukherjee A (2016) Catechol oxidase and phenoxazinone synthase: biomimetic functional models and mechanistic studies. *Coord Chem Rev* 310:80–115. <https://doi.org/10.1016/j.ccr.2015.11.002>
- Abu-Dief AM, Mohamed IMA (2015) A review on versatile applications of transition metal complexes incorporating Schiff bases. *Beni Suef Univ J Basic Appl Sci* 4:119–133. <https://doi.org/10.1016/j.bjbas.2015.05.004>
- Madalan AM, Ene CD (2018) Supramolecular rectangles and ladders constructed from Ni(II), Cu(II) and Zn(II) mononuclear complexes with bicompartamental ligands and 4-aminopyridine as tectons. *Inorg Chim Acta* 475:184–192. <https://doi.org/10.1016/j.ica.2017.06.058>
- Cozzi PG (2004) Metal–Salen Schiff base complexes in catalysis: practical aspects. *Chem Soc Rev* 33:410–421. <https://doi.org/10.1039/B307853C>
- Finelli A, Héroult N, Crochet A, Fromm KM (2018) Threading Salen-type Cu- and Ni-complexes into one-dimensional coordination polymers: solution versus solid state and the size effect of the alkali metal ion. *Cryst Growth Des* 18:1215–1226. <https://doi.org/10.1021/acs.cgd.7b01769>
- Eicken C, Zippel F, Büldt-Karentzopoulos K, Krebs B (1998) Biochemical and spectroscopic characterization of catechol oxidase from sweet potatoes (*Ipomoea batatas*) containing a type-3 dicopper center 1. *FEBS Lett* 436:293–299. [https://doi.org/10.1016/S0014-5793\(98\)01113-2](https://doi.org/10.1016/S0014-5793(98)01113-2)
- Rompel A, Fischer H, Meiwes D et al (1999) Substrate specificity of catechol oxidase from *Lycopus europaeus* and characterization

- of the bioproducts of enzymic caffeic acid oxidation I. FEBS Lett 445:103–110. [https://doi.org/10.1016/S0014-5793\(99\)00106-4](https://doi.org/10.1016/S0014-5793(99)00106-4)
14. Thakurta S, Chakraborty J, Rosair G et al (2009) The interplay of O–H···O hydrogen bonding in the generation of three new supramolecular complexes of Cu^{II}, Ni^{II} and Co^{III}: Syntheses, characterization and structural aspects. Inorg Chim Acta 362:2828–2836. <https://doi.org/10.1016/j.ica.2009.01.002>
 15. Gomes L, Sousa C, Freire C, de Castro B (2000) Diaqua{6,6'-dimethoxy-2,2'-[propane-1,3-diy]bis(nitrilomethylidyne-N)}diphenolato-O, O'}nickel(II). Acta Crystallogr Sect C Cryst Struct Commun 56:1201–1203. <https://doi.org/10.1107/S010827010001009X>
 16. Thakurta S, Butcher RJ, Gómez-García CJ et al (2010) Synthesis, structural aspects and magnetic properties of an unusual 2D thiocyanato-bridged cobalt(II)–Schiff base network. Inorg Chim Acta 363:3981–3986. <https://doi.org/10.1016/j.ica.2010.07.069>
 17. Basak T, Ghosh K, Gómez-García CJ, Chattopadhyay S (2018) Synthesis, structure and magnetic characterization of a dinuclear and two mononuclear iron(III) complexes with N, O-donor Schiff base ligands. Polyhedron 146:42–54. <https://doi.org/10.1016/j.poly.2017.12.040>
 18. Banerjee S, Saha A (2016) A new end-on (μ -1,1) azido bridged [Zn₂(L)₂(Na)N₃]_n 1D chain derived from a trinuclear zinc complex: syntheses, crystal structures, photoluminescence properties and DFT study. J Coord Chem 69:3092–3106. <https://doi.org/10.1080/00958972.2016.1226502>
 19. Banerjee S, Ghorai P, Sarkar P et al (2020) A rare flattened tetrahedral Mn(II) salen type complex: synthesis, crystal structure, biomimetic catalysis and DFT study. Inorg Chim Acta 499:119176. <https://doi.org/10.1016/j.ica.2019.119176>
 20. Biswas D, Chakrabarty PP, Saha S et al (2013) Ligand mediated structural diversity and role of different weak interactions in molecular self-assembly of a series of copper(II)–sodium(I) Schiff-base heterometallic complexes. Inorg Chim Acta 408:172–180. <https://doi.org/10.1016/j.ica.2013.09.011>
 21. Chiboub Fella FZ, Costes J-P, Dahan F et al (2007) Varying the metal/metal ratio in related Cu–Ca complexes. Polyhedron 26:4209–4215. <https://doi.org/10.1016/j.poly.2007.05.019>
 22. Branzea DG, Madalan AM, Ciattini S et al (2010) New heterometallic coordination polymers constructed from 3d–3d' binuclear nodes. New J Chem 34:2479. <https://doi.org/10.1039/c0nj00238k>
 23. Cai X, Ning H (2015) Crystal structure of di- μ -acetato-diacetato-bis(μ -6,6'-dimethoxy-2,2'-{[(propane-1,3-diy]bis(azanylylidene)}bis(methanylylidene)}diphenolato) tetrazinc. Acta Crystallogr Sect E Crystallogr Commun 71:m217–m218. <https://doi.org/10.1107/S2056989015020551>
 24. Wang J-H, Yan P-F, Li G-M et al (2010) *N,N'*-Bis(2-hydroxy-3-methoxybenzylidene)-1,3-diaminopropane dimeric 4f and 3d–4f heterodinuclear complexes: syntheses, crystal structures and magnetic properties. Inorg Chim Acta 363:3706–3713. <https://doi.org/10.1016/j.ica.2010.05.030>
 25. Lee JH, Im SY, Lee SW (2018) Pd–Ln and Pt–Ln complexes of a bi-compartmental ligand: [MLn(L)(NO₃)₃] (M = Pd, Pt; Ln = Eu, Tb; H₂L = *N,N'*-bis(3-methoxysalicylideneimino)-1,3-diaminopropane). Inorg Chim Acta 474:89–95. <https://doi.org/10.1016/j.ica.2018.01.020>
 26. Pasatoiu TD, Ghirri A, Madalan AM et al (2014) Octanuclear [Ni^{II}₄Ln^{III}₄] complexes. Synthesis, crystal structures and magnetocaloric properties. Dalton Trans 43:9136–9142. <https://doi.org/10.1039/C4DT00515E>
 27. Wang H (2009) Aqua {6,6'-dimethoxy-2,2'-[propane-1,3-diy]bis(nitrilomethylidyne)}diphenolato}copper(II). Acta Crystallogr Sect E Struct Rep Online 65:m1490–m1490. <https://doi.org/10.1107/S1600536809042755>
 28. Roy S, Basak T, Khan S et al (2017) A combined experimental and theoretical study on the formation of a cyclic tetrameric water cluster and a similar type of cyclic cluster in copper(II) Schiff base complexes. Chem Sel 2:9336–9343. <https://doi.org/10.1002/slct.201701266>
 29. Cucos A, Ursu A, Madalan AM et al (2011) Co-crystallization of coordination compounds through second-coordination sphere interactions. CrystEngComm 13:3756. <https://doi.org/10.1039/c1ce05112a>
 30. Routaray A, Nath N, Maharana T, Kumar AS (2015) Synthesis and immortal ROP of L-lactide using copper complex. J Macromol Sci Part A 52:444–453. <https://doi.org/10.1080/10601325.2015.1029370>
 31. Sheldrick GM (2015) SHELXT—Integrated space-group and crystal-structure determination. Acta Crystallogr Sect A Found Adv 71:3–8. <https://doi.org/10.1107/S2053273314026370>
 32. Dolomanov OV, Bourhis LJ, Gildea RJ et al (2009) OLEX2: a complete structure solution, refinement and analysis program. J Appl Crystallogr 42:339–341. <https://doi.org/10.1107/S0021898008042726>
 33. Routaray A, Nath N, Maharana T et al (2016) Salicylaldehyde Copper(II) complex catalyst: pioneer for ring opening polymerization of lactide. J Chem Sci 128:883–891. <https://doi.org/10.1007/s12039-016-1091-3>
 34. Nakamoto K (2008) Infrared and Raman spectra of inorganic and coordination compounds. Wiley, Hoboken, pp 1–273. <https://doi.org/10.1002/9780470405888.ch1>
 35. Maurya RC, Patel P, Rajput S (2003) Synthesis and characterization of *N*-(*o*-Vanillinidene)-*p*-anisidine and *N,N'*-bis(*o*-Vanillinidene)ethylenediamine and their metal complexes. Synth React Inorg Met Chem 33:817–836. <https://doi.org/10.1081/SIM-120021648>
 36. Banu KS, Mukherjee M, Guha A et al (2012) Dinuclear copper(II) complexes: solvent dependent catecholase activity. Polyhedron 45:245–254. <https://doi.org/10.1016/j.poly.2012.06.087>
 37. Chattopadhyay T, Mukherjee M, Mondal A et al (2010) A unique nickel system having versatile catalytic activity of biological significance. Inorg Chem 49:3121–3129. <https://doi.org/10.1021/ic901546t>
 38. Banu KS, Chattopadhyay T, Banerjee A et al (2008) Catechol oxidase activity of a series of new dinuclear copper(II) complexes with 3,5-DTBC and TCC as substrates: syntheses, X-ray crystal structures, spectroscopic characterization of the adducts and kinetic studies. Inorg Chem 47:7083–7093. <https://doi.org/10.1021/ic701332w>
 39. Banu KS, Chattopadhyay T, Banerjee A et al (2009) Catechol oxidase activity of dinuclear copper(II) complexes of Robson type macrocyclic ligands: syntheses, X-ray crystal structure, spectroscopic characterization of the adducts and kinetic studies. J Mol Catal A Chem 310:34–41. <https://doi.org/10.1016/j.molcata.2009.05.016>
 40. Adak P, Mondal A, Chattopadhyay SK (2020) Manganese(II) complex of an oxygen–nitrogen donor Schiff base ligand showing efficient catechol oxidase activity: synthesis, spectroscopic and kinetic study. New J Chem 44:3748–3754. <https://doi.org/10.1039/C9NJ04591K>
 41. Solomon EI, Sundaram UM, Machonkin TE (1996) Multicopper oxidases and oxygenases. Chem Rev 96:2563–2606. <https://doi.org/10.1021/cr950046o>
 42. Güell M, Siegbahn PEM (2007) Theoretical study of the catalytic mechanism of catechol oxidase. JBIC J Biol Inorg Chem 12:1251–1264. <https://doi.org/10.1007/s00775-007-0293-z>
 43. Kaizer J, Baráth G, Csonka R et al (2008) Catechol oxidase and phenoxazinone synthase activity of a manganese(II) isoindoline complex. J Inorg Biochem 102:773–780. <https://doi.org/10.1016/j.jinorgbio.2007.11.014>

44. Blay G, Fernández I, Pedro JR et al (2006) Chemistry and reactivity of dinuclear manganese oxamate complexes: aerobic catechol oxidation catalyzed by high-valent bis(oxo)-bridged dimanganese(IV) complexes with a homologous series of binucleating 4,5-disubstituted-o-phenylenedioxamate ligands. *J Mol Catal A Chem* 250:20–26. <https://doi.org/10.1016/j.molcata.2006.01.021>
45. Hitomi Y, Ando A, Matsui H et al (2005) Aerobic catechol oxidation catalyzed by a Bis(μ -oxo)dimanganese(III, III) complex via a manganese(II)–semiquinonate complex. *Inorg Chem* 44:3473–3478. <https://doi.org/10.1021/ic050109d>
46. Mukherjee S, Weyhermüller T, Bothe E et al (2004) Dinuclear and mononuclear manganese(IV)–radical complexes and their catalytic catecholase activity. *Dalton Trans.* <https://doi.org/10.1039/B410842F>
47. Doctrow SR, Huffman K, Marcus CB et al (2002) Salen–manganese complexes as catalytic scavengers of hydrogen peroxide and cytoprotective agents: structure–activity relationship studies. *J Med Chem* 45:4549–4558. <https://doi.org/10.1021/jm020207y>
48. Prasad RV, Thakkar NV (1994) Study of cobalt complexes as catalysts in the decomposition of hydrogen peroxide. *J Mol Catal* 92:9–20. [https://doi.org/10.1016/0304-5102\(94\)00063-8](https://doi.org/10.1016/0304-5102(94)00063-8)

Publisher's Note Springer Nature remains neutral with regard to jurisdictional claims in published maps and institutional affiliations.

Affiliations

Aarón Terán¹  · Aida Jaafar¹ · Ana E. Sánchez-Peláez¹ · M. Carmen Torralba¹ · Ángel Gutiérrez¹

✉ Aarón Terán
aaronter@ucm.es

¹ Departamento de Química Inorgánica, Facultad de Ciencias Químicas, Universidad Complutense de Madrid, 28040 Madrid, Spain